A Platinum Open Access Journal for Organic Chemistry

Paper

Free to Authors and Readers | DOAJ Seal | *Arkivoc* **2023** (ii) 202312013

New phenyldibenzophosphole oxide-based acceptors for blue exciplex-forming systems

Chun-Yen Lin[1], Yu-Neng Chen[1], Cheng-Kai Wang[2], Wen-Yi Hung[2,*], Ken-Tsung Wong[1,3*]

[1]*Department of Chemistry, National Taiwan University, Taipei 10617, Taiwan*
[2]*Department of Optoelectronics and Materials Technology, National Taiwan Ocean University, Keelung 202, Taiwan*
[3]*Institute of Atomic and Molecular Sciences, Academia Sinica, Taipei 10617, Taiwan*
Email: wenhung@mail.ntou.edu.tw; kenwong@ntu.edu.tw

This article is dedicated to Professor Tien-Yau Luh for his contributions to chemical education and research

Received 05-02-2023 **Accepted Manuscript** 10-26-2023 **Published on line** 11-06-2023

Abstract

The exciplex-forming system occurred at the donor -acceptor interface that can emit deep blue emission is still very rare due to the scarcity of appropriate donor and acceptor molecules. The design, synthesis and characterizations of two phenyldibenzophosphole oxide-based acceptors with para- and meta-substituted benzonitrile peripherals for fine-tuning the frontier orbitals are reported. With suitably selected indenocarbazole-based donors, blue to deep blue exciplex-forming systems with thermally activated delayed fluorescence were identified and verified by time-resolved photoluminescence.

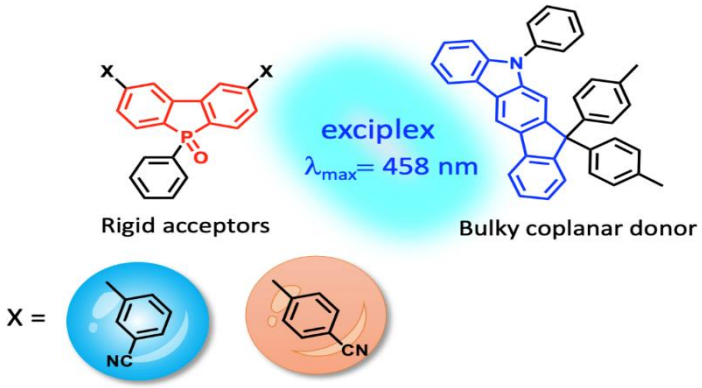

Keywords: Thermally-activated delayed fluorescence, exciplex, rigid acceptor, deep blue emission, phosphole, synthesis

Introduction

Pure organic emitters that can give off thermally activated delayed fluorescence (TADF) have become the key to achieve high efficiency organic light-emitting diodes (OLEDs).[1-3] The efficiency of the TADF emitters employed in OLED device relies on the molecularly-engineered structure to minimize the singlet-triplet energy gap (ΔE_{ST}) for up-converting triplet excitons back to singlet state to attain 100% internal quantum efficiency (IQE) via reverse intersystem crossing (rISC) process.[4] In order to achieve small ΔE_{ST}, some molecular design strategies have been developed, including the tailor-made molecules that can subtly perform through bond or through space intramolecular charge transfer (ICT).[5-7] Nowadays, the TADF emitters based on ICT approach have been witnessed to be very successful for boosting the external quantum efficiency (EQE) up to more than 36%.[8-12] In addition to the molecular TADF systems, the physically mixed donor (D)-acceptor (A) blends generating exciplex via intermolecular charge transfer at the D/A interface are also effective for creating TADF emission.[13, 14] The emission of exciplex-forming system could be feasibly tuned through physical mixing of carefully designed D and A molecules. For the exciplex exciton, the highest occupied molecular orbital (HOMO) would be mainly localized on the D molecule and the lowest unoccupied molecular orbital (LUMO) would mainly be situated on the A molecule, leading to negligible ΔE_{ST} for efficient rISC. The exciplex systems with TADF are of myriad advantages such as flexible emission tunability, easy synthesis, and simplified device structures, and versatile utilizations, making exciplex-forming systems be important in the materials development of OLED.[15] After one decade endeavor, the EQEs of exciplex-based OLEDs have been reported to achieve better than 20%.[16] Nevertheless, the exciplex-forming blends often suffer from weak transition dipole, leading to low photoluminescence quantum yield (PLQY) and thus inferior device efficiency.[17, 18] Furthermore, exciplex system that can give off deep blue emission is still very rare due to the scarcity of suitable D and A molecules. Hence, there is still demand to develop more reliable deep blue exciplex system by careful molecular design strategy.

To develop blue exciplex system, the frontier orbitals of the donor and acceptor should be judiciously modified for creating sufficient energy barriers for accumulating the holes and electrons at the D/A interface. In addition, the triplet energy of the components needs to be as high as ~2.75 eV for confining the excitons on the exciplex, rendering the development of blue exciplex-forming system particularly challenging. The carbazole-based, molecules are often reported as donors to mix with phosphine oxide-based acceptors for giving blue exciplexes. For example, in 2014, Hung *et. al.* reported a sky blue exciplex system comprising mCP as donor and PO-T2T as acceptor. The EQE of the mCP:PO-T2T-based OLED device can reach as high as 8%.[19] In 2017, Lim *et. al.* developed a deep blue exciplex system incorporated mCP as donor and triphenyl phosphine-oxide based BM-A10 as acceptor.[20] The emission wavelength of the mCP:BM-A10 exciplex system can be fine-tuned to 455 nm. In 2018, Lin *et. al.* reported the use of CN-Cz2 as donor and PO-T2T as acceptor to achieve the sky-blue exciplex emission (PL λ_{max} = ~490 nm)[21], and OLED device based on CN-Cz2:PO-T2T can achieve an EQE of 16%.[21] According to the reported literatures, phosphine oxide-based acceptors possess high potential toward the development of efficient sky blue to blue exciplex-forming systems, however, such exciplex system with high device efficiency is still pending. Hence, it is essential to propose a new molecular design strategy to simultaneously modulate the energy level and enhance the exciplex PLQY.

In 2019, Zhong *et. al.* reported the use of phenyldibenzophosphole oxide as the electron-accepting group to develop a series of donor-π-acceptor (D-p-A) type molecular TADF emitters.[22] It is found out that the fused five-membered phosphine oxide ring can lock the molecular conformation and enhance the rigidity of the emitter, leading to enhanced OLED device performances as compared to that of the counter device employing the emitters with free-form phosphine oxide. Based on this report, we envision that the phenyldibenzophosphole oxide moiety might be a good solution to enhance the efficiency of deep blue exciplex

systems. In this work, we report the design and synthesis of two phenyldibenzophosphole oxide-based acceptors, namely **p-CNPO** and **m-CNPO**. The para- and meta-substituted benzonitrile peripherals introduced on phenyldibenzophosphole oxide core to respectively make **p-CNPO** and **m-CNPO** are anticipated to fine-tune the frontier orbitals and the electron transport of the molecules. The electrochemical and photophysical properties of **p-CNPO** and **m-CNPO** support their potential for blue exciplex-forming systems with suitably selected carbazole-based donors. Hence, we adopted the aggregation induced emission (AIE) approach[23] as a quick scan platform for finding the suitable donors. Based on this method, we found two indenocarbazole-based donor molecules, namely **i-ICz** and **o-ICz**, can afford the blue to deep blue exciplex-forming systems. Among which, the vacuum co-deposited **o-ICz**:**m-CNPO** blend film exhibits intense TADF exciplex emission centered at 458 nm with a PLQY of 11%. Although the efficiency still has room to be improved, this work demonstrates the potential of dibenzophosphole-based acceptor toward efficient deep blue exciplex-forming system that might trigger new innovative molecular design strategy of acceptor for high-energy exciplex-forming systems.

Results and Discussion

The chemical structure and synthetic route of the four targeted compounds, namely **p-CNPO**, **m-CNPO**, **i-ICz**, and **o-iCz** are depicted in Scheme 1. As depicted in Scheme 1, **p-CNPO** and **m-CNPO** were prepared by reacting the reported precursor **3**[22] with the corresponding para- and meta-benzonitrile pinacolborane derivatives under a typical Suzuki coupling condition. On the other hand, **i-ICz** and **o-ICz** were synthesized following the protocol reported by us.[24] The cyclization precursor **2** was obtained by the treatment of **1** with the corresponding Grignard reagent. Subsequently, **2** was underwent an intramolecular Friedel-Crafts cyclization catalyzed by HCl/AcOH to afford pure titled compound **i-ICz**. Interestingly, when pure HCl was directly added to **2**, **i-ICz** and **o-ICz** were obtained simultaneously with a molar ratio of ~1:0.3. All the target molecules were purified with column chromatography and vacuum sublimation, and then fully characterized by ^{1}H and ^{13}C NMR spectroscopy and mass spectrometry.

Cyclic voltammetry (CV) was carried out to probe the electrochemical properties of **p-CNPO**, **m-CNPO**, **i-ICz**, and **o-ICz**, respectively (Table 1 and Figure 1). The reduction potentials of **p-CNPO** and **m-CNPO** are -1.36 V and -1.45 V, respectively. The LUMO energy levels are calculated based on the reduction half-wave potentials referring to ferrocene/ferrocenium (Fc/Fc^{+}) redox couple, and the corresponding LUMO energy levels of **p-CNPO** and **m-CNPO** are calculated as -2.84 eV and -2.75 eV, respectively. The slightly lower LUMO energy level of **p-CNPO** with respect to that of **m-CNPO** suggests that the electronic property depends to the CN-position of the benzonitrile substituent. The low LUMO energy levels of **p-CNPO** and **m-CNPO** indicate their potential for acting as electron acceptor. The HOMO energy level for **p-CNPO** and **m-CNPO** are estimated by the subtract of their LUMO energy level and optical energy gap (LUMO - E_g) as -6.76 eV and -6.69 eV, respectively. The oxidation potentials of **i-ICz** and **o-ICz** are 1.20 V and 1.26 V, respectively. The HOMO energy levels are calculated based on the oxidation half-wave potentials referring to ferrocene/ferrocenium (Fc/Fc^{+}) redox couple, and the corresponding HOMO energy levels of **i-ICz** and **o-ICz** are calculated as -5.45 eV and -5.51 eV, respectively. The slightly higher HOMO energy level of **i-ICz** with respect to that of **o-ICz** suggests the electron-donating ability of the indenocarbazole core could be modified by the C-bridge position of fluorene. The high HOMO energy levels of **i-ICz** and **o-ICz** indicate their potential for acting as an electron donor. The LUMO energy level for **i-ICz** and **o-ICz** are estimated to be -2.20 eV and -2.23 eV, respectively, using the sum of their HOMO energy level and optical energy gap (HOMO + E_g). The good energy level alignment of the ICz donors and CNPO acceptors indicate their potential for giving exciplex emission.

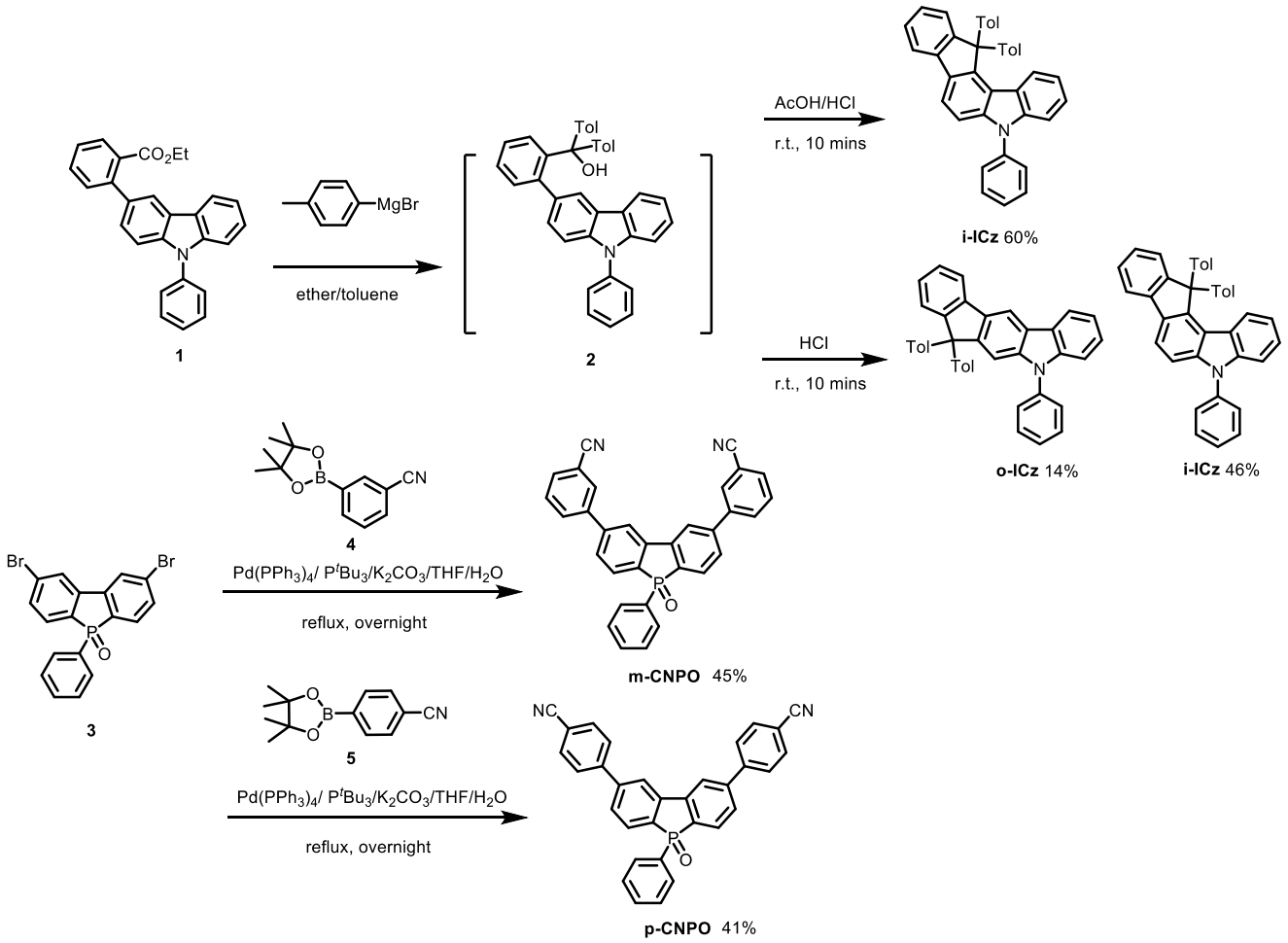

Scheme 1. The synthetic route and chemical structure of **i-ICz**, **o-ICz**, **p-CNPO**, and **m-CNPO**.

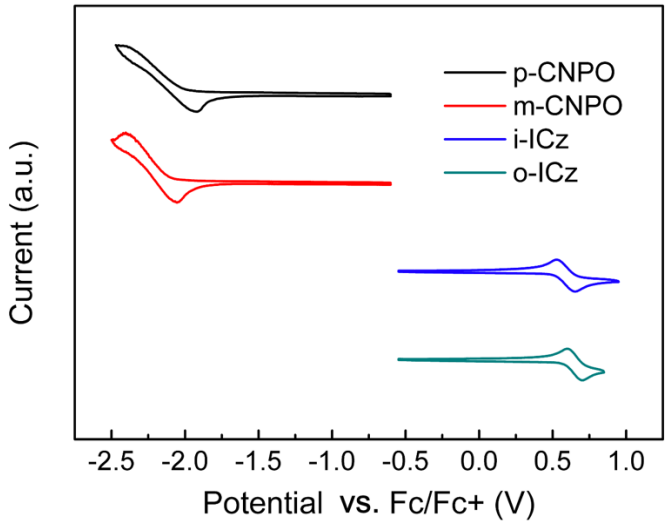

Figure 1. Cyclic voltammetry of **p-CNPO**, **m-CNPO**, **i-ICz**, and **o-ICz**.

To study the photophysical properties of the newly prepared ICz donors and CNPO acceptors in solution, the electronic absorption (UV-Vis) and photoluminescence (PL) of **p-CNPO**, **m-CNPO**, **i-ICz**, and **o-ICz** measured in toluene solutions are depicted in Figure 2 and the data are summarized in Table 1. As shown in Figure 2(a), the absorption bands for **p-CNPO** and **m-CNPO** appeared around 270 nm, and the slightly bathochromic shift of **p-CNPO** absorption as compared to that of **m-CNPO** indicates its higher conjugation due to the para-substituted benzonitrile group. The weak absorption bands around 340~380 nm of **i-ICz** and **o-ICz** can be attributed to the n to π^* transition of the carbazole moiety[25], and the strong absorption bands around 280~320 nm can be ascribed to the π to π^* absorption of the molecules. Interestingly, the isomeric effect of fluorene C-bridge position of **i-ICz** and **o-ICz** leads to different π to π^* absorption. The more structured absorption peak of **i-ICz** as compared to that of **o-ICz** suggests its higher rigidity. As depicted in Figure 2(b), the fluorescence peak of **p-CNPO** and **m-CNPO** is around 390 nm. On the other hand, the fluorescence peaks of **i-ICz** and **o-ICz** are centered at around 380~390 nm. The more structured and slightly narrower emission for **i-ICz** with respect to that of **o-ICz** once again elucidates its higher molecular rigidity. Furthermore, the Stoke shifts of the CNPO acceptors are larger than those of the ICz based donors. This indicates that the indenocarbazole-based donors possess smaller reorganization energy due to its C- and N-locked molecular rigidity.

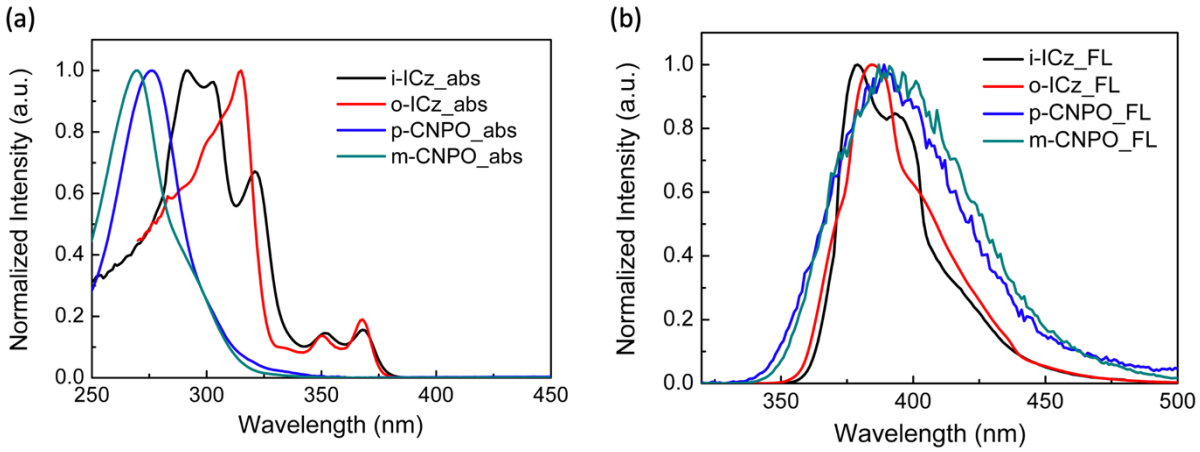

Figure 2. (a) UV-vis and (b) Photoluminescence spectra of **p-CNPO**, **m-CNPO**, **i-ICz**, and **o-ICz** measured in toluene solutions (1×10^{-5} M).

Table 1. Summary of the photophysical and electrochemical data for **p-CNPO**, **m-CNPO** and the various donors

	λ_{abs} (nm)[a]	λ_{FL} (nm)[b]	E_g (eV)[c]	HOMO (eV)	LUMO (eV)
i-ICz	352/368	378/394	3.25	-5.45[d]	-2.20[f]
o-ICz	350/367	384	3.28	-5.51[d]	-2.23[f]
BCzPh[26]	303	391/408	3.37	-5.67	-2.30
BCz3Ph[27]	305	406	3.34	-5.22	-1.88
BCz4Ph[28]	305	408	3.34	-5.31	-1.97
p-CNPO	269	390	3.94	-6.76[g]	-2.84[e]
m-CNPO	276	393	3.92	-6.69[g]	-2.75[e]

a. absorption maxima wavelength obtained in toluene solution (1×10^{-5}M); b. Fluorescence max. wavelength; c. Energy gap calculated from onset of UV-Vis spectra; d. HOMO level calculated from oxidation half-wave potential using cyclic voltammetry; e. LUMO level calculated from oxidation half-wave potential using cyclic voltammetry; f. LUMO level calculated from HOMO+E_g; g. HOMO level calculated from LUMO-E_g

For probing the exciplex formation, we utilized aggregation induced emission (AIE) method[23] to scan the suitable donors for **p-CNPO** and **m-CNPO**. In addition to **i-ICz** and **o-ICz** donors, three biscarbazole derivatives have been examined and their capability of formation exciplex with **p-CNPO** and **m-CNPO** has been investigated. The physical properties of biscarbazole-based donors are summarized in Table 1. By slowly adding the respective THF solution of donor (D) and acceptors **p-CNPO** and **m-CNPO** into distilled water, followed by sonification for 3 minutes to remove the THF, the D:**p-CNPO** and D:**m-CNPO** nanoparticles (NPs) were prepared for the PL measurement. As depicted in Figure 3, all the donors blended with **p-CNPO** and **m-CNPO** could form red-shifted and structureless fluorescence respectively, revealing the signature of excipex formation from their intermolecular charge transfer states. Obviously, the D/A-blended NPs with biscarbazole-based donors exhibit red-shifted emission as compared to those of NPs with indenocarbazole-based donors, agreeing with the higher HOMOs of biscarbazole. However, the appearance of the residual emission from components indicates the insufficient exciplex formation between CNPO acceptors and biscarbazole-based donors. Intriguingly, the lower HOMOs of **i-ICz** and **o-ICz** leads the **CNPO-** and **m-CNPO**-blended NPs to exhibit blue emission without the least residual emission of donors and acceptors. This AIE approach reveals the better propensity of forming exciplex with CNPO acceptors.

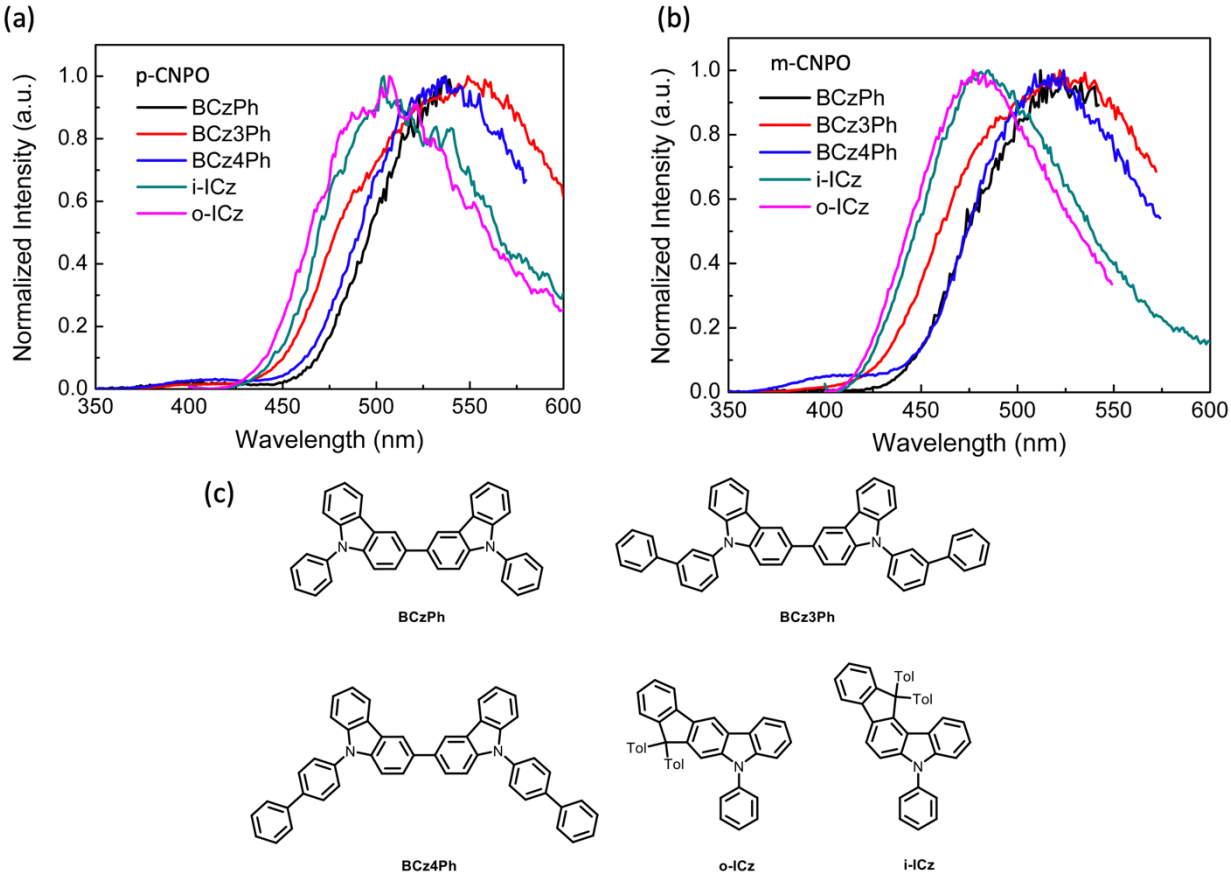

Figure 3. The PL spectra of D/A-blended NPs formed by using acceptor **p-CNPO** (a) and **m-CNPO** (b) with the various donors, (c) the chemical structures of the donors using for AIE test.

The electrochemical, photophysical, and AIE screening indicate that the ICz donors and the CNPO acceptors could achieve exciplex emission. Hence, the vacuum co-deposited blending films of **i-ICz**:**p-CNPO**, **i-ICz**:**m-CNPO**, **o-ICz**:**p-CNPO**, and **o-ICz**:**m-CNPO** (1:1 by weight) were prepared and examined for the exciplex properties. The data are summarized in Table 2. As depicted in Figure 4, all the four blend films exhibit red-shifted and structureless emission. To further verify the TADF feature of the new emissions, the time-resolved photoluminescence (TrPL) of the four blend films were measured. The TrPL results indicate the emissions composed of a pump and a delayed component, corroborating their TADF properties. As noticed, the blend films incorporated **o-ICz** as donors (**o-ICz**:**p-CNPO** and **o-ICz**:**m-CNPO**) exhibit faster prompt and delay fluorescence lifetime as compared to those of **i-ICz** based blend films (**i-ICz**:**p-CNPO** and **i-ICz**:**m-CNPO**). This result indicates that the exciton recombination is more efficient of **o-ICz**:**p-CNPO** and **o-ICz**:**m-CNPO films** with respect to those of **i-ICz**:**p-CNPO** and **i-ICz**:**p-CNPO** films. Accordingly, **o-ICz**-based blend films have higher PLQYs than **i-ICz**-based blend films (**o-ICz**:**p-CNPO** (15%) vs. **i-ICz**:**p-CNPO** (12%); **o-ICz**:**m-CNPO** (11%) vs. **i-ICz**:**m-CNPO** (10%)). The low PLQYs for these exciplex systems might be attributed to the low transition dipole that lead to small radiative decay rate. More importantly, **o-ICz**-based blend films show blue-shifted exciplex emission as compared to those of counterpart films formed by the **i-ICz**-based blend films (**o-ICz**:**p-CNPO** (487 nm) vs. **i-ICz**:**p-CNPO** (500 nm); **o-ICz**:**m-CNPO** (458 nm) vs. **i-ICz**:**m-CNPO** (502 nm)). This phenomenon can be attributed to the lower HOMO of **o-ICz**. However, the position of the two tolyl peripheral groups of **o-ICz** that can lead to longer D-A distances may also blue-shift the exciplex emission.[29] In addition, the **o-ICz**:**p-CNPO** blended film exhibits obvious red-shifted exciplex emission (487 nm) as compared to that (458 nm) of **the o-ICz**:**m-CNPO** film, which is reasonable

due to the lower LUMO for **p-CNPO**. Nevertheless, the emission of **i-ICz**:**p-CNPO** (500 nm) and **i-ICz**:**m-CNPO** (502 nm) films show similar exciplex emission peak and comparable PLQY. This might result from the combining effects of molecular energy levels and the D-A distances of **i-ICz**:**p-CNPO** and **i-ICz**:**m-CNPO** films.

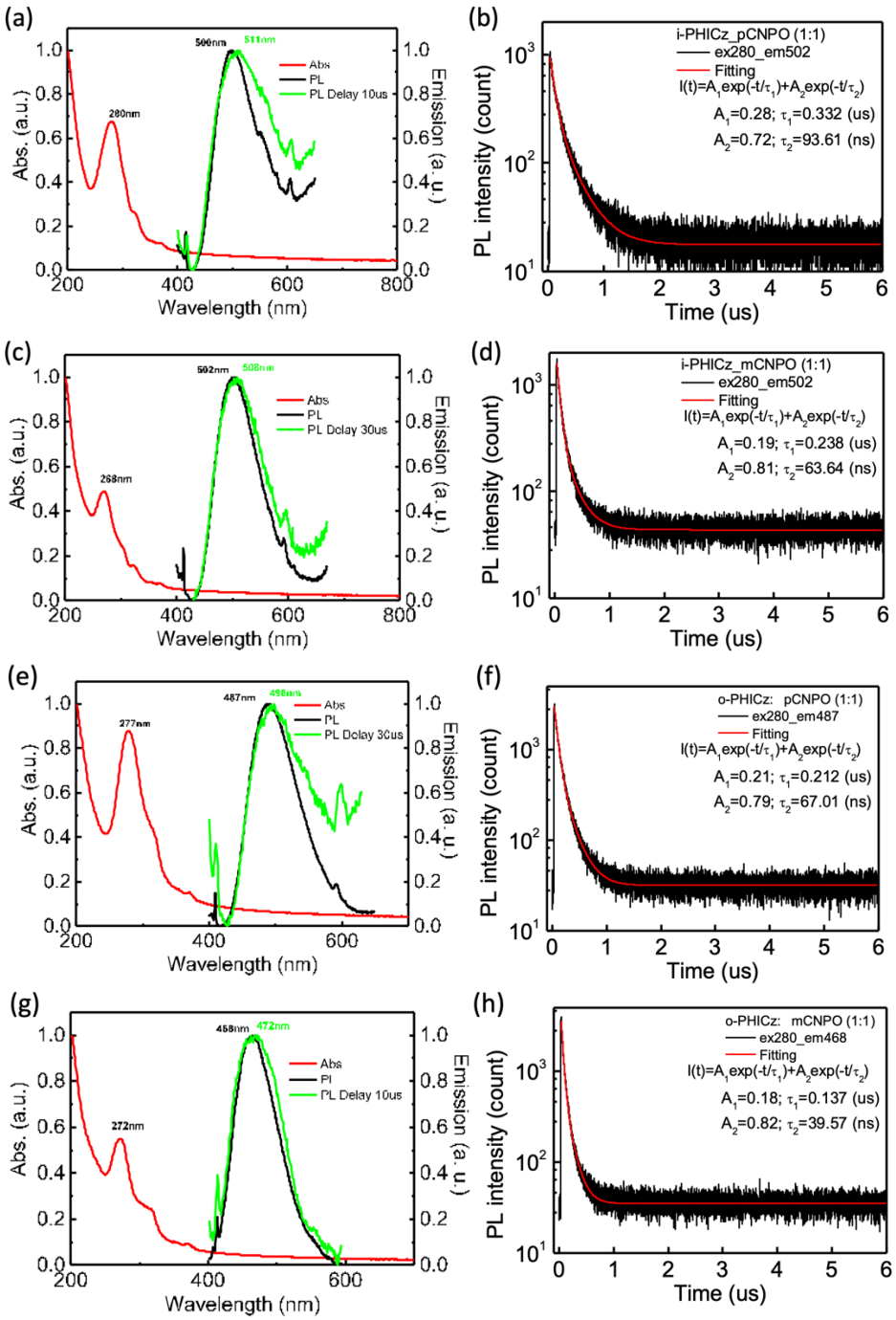

Figure 4. The absorption and photoluminescence spectra of the blend films (a) **i-ICz**:**p-CNPO**, (b) **i-ICz**:**m-CNPO**, (c) **o-ICz**:**p-CNPO**, and (d) **o-ICz**:**m-CNPO**, and the time-resolved photoluminescence spectra (TrPL) of the blend films (b) **i-ICz**:**p-CNPO**, (d) **i-ICz**:**m-CNPO**, (f) **o-ICz**:**p-CNPO**, and (h) **o-ICz**:**m-CNPO**.

Table 2. The photophysical data summary of the D:A blend films **i-ICz**:**p-CNPO**, **i-ICz**:**m-CNPO**, **o-ICz**:**p-CNPO**, and **o-ICz**:**m-CNPO**

Donor: acceptor (1:1)	PF (ns)[a]	DF (ms)[b]	PLQY (%)[c]	Emission (nm)
i-ICz : p-CNPO	93.61	0.332	12	500
i-ICz : m-CNPO	63.64	0.238	10	502
o-ICz : p-CNPO	67.01	0.212	15	487
o-ICz : m-CNPO	39.57	0.137	11	458

a. prompt fluorescence lifetime; b. delay fluorescence lifetime; c. photoluminescence quantum yield of the blend films.

Conclusions

In summary, two phenyldibenzophosphole oxide-based acceptors, **p-CNPO** and **m-CNPO** are designed and synthesized. The para- and meta-substituted benzonitrile peripherals modified on phenyldibenzophosphole oxide core are capable to fine-tune the frontier orbitals of **p-CNPO** and **m-CNPO**. The electrochemical and photophysical properties of **p-CNPO** and **m-CNPO** support their potential toward blue exciplex-forming systems with carefully selected carbazole-based donors. Adopting the aggregation induced emission (AIE) approach as a quick scan platform for selecting the suitable donors, two indenocarbazole-based donor molecules, **i-ICz** and **o-ICz**, were found to afford the blue to deep blue exciplex-forming systems. The **i-ICz**:**p-CNPO**, **i-ICz**:**m-CNPO**, **o-ICz**:**p-CNPO**, and **o-ICz**:**m-CNPO** blend films were fabricated to investigate their solid state TADF properties. Among them, the vacuum co-deposited **o-ICz**:**m-CNPO** blend film exhibits intense exciplex emission centered at 458 nm with a PLQY of 11%. The exciplex emission was examined by time-resolved photoluminescence to verifiy the TADF character. The molecular design strategy paves a new way for potential acceptors that can achieve efficient deep blue exciplex OLEDs in the future.

Experimental Section

*Synthesis of 3,3'-(5-oxido-5-phenylbenzo[b]phosphindole-2,8-diyl)dibenzonitrile (**m-CNPO**)*

3 (2.17 g, 5.00mmol), **4** (2.5 g, 10.92 mmol), $Pd(PPh_3)_4$ (580 mg, 0.50 mmol), and K_2CO_3 (4.14 g, 30 mmol) were placed in a reaction flask, followed by adding P^tBu_3 (0.05M in toluene, 40 mL), THF (250 mL), and water (5 mL) under an argon atmosphere. The reaction was kept at 90°C overnight and then extracted with EtOAc and brine. The resulting organic layer was dried over $MgSO_4$ and the solvent was removed by rotavapor. The crude product was then purified by column chromatography (CH_2Cl_2/EtOAc = 3/1) to afford **m-CNPO** as white solid (1.08 g, 45%). mp: 270-272 °C. ^{1}H NMR (400 MHz, $CDCl_3$) δ (ppm) 8.07 (s,2H), 7.98 (s, 2H), 7.94-7.84 (m, 4H), 7.75-7.69 (m, 4H), 7.66-7.61 (m, 4H), 7.58-7.53 (m, 1H), 7.47-7.42 (m, 2H). ^{13}C NMR (101 MHz, $CDCl_3$) δ (ppm) 144.3, 142.4, 142.2, 141.2, 133.8, 132.7, 132.5, 131.7, 130.9, 130.0, 128.8, 120.0, 118.4, 113.4. ^{31}P NMR (162 MHz, $CDCl_3$) δ (ppm) 33.640. HRMS (MALDI-TOF, *m/z*) calcd for $C_{32}H_{19}N_2OP[M+H]^+$, 479.1313, found 479.1327.

*Synthesis of 4,4'-(5-oxido-5-phenylbenzo[b]phosphindole-2,8-diyl)dibenzonitrile (**p-CNPO**)*

3 (2.17 g, 5.00mmol), **5** (2.5 g, 10.92 mmol), $Pd(PPh_3)_4$ (580 mg, 0.50 mmol), and K_2CO_3 (4.14 g, 30 mmol) were placed in a reaction flask, followed by adding P^tBu_3 (0.05M in toluene, 40 mL), THF (250 mL), and water (5 mL) under an argon atmosphere. The reaction was kept at 90°C overnight and then extracted with EtOAc and brine. The resulting organic layer was dried over $MgSO_4$,and the solvent was removed by rotavapor. The crude product was then purified by column chromatography (CH_2Cl_2/EtOAc = 3/1) to afford **p-CNPO** as white solid (982 mg, 41%). mp: 338-340 °C. ^{1}H NMR (400 MHz, $CDCl_3$) δ (ppm) 8.07 (s, 2H), 7.88-7.77 (m, 10H), 7.74-7.68 (m, 2H) 7.65-7.63 (m, 2H) 7.55 (m, 1H) 7.47-7.42 (m, 2H). ^{13}C NMR (101 MHz, $CDCl_3$) δ (ppm) 144.7, 144.3, 142.3, 142.1, 132.8, 132.6, 131.1, 130.7, 129.0, 128.0, 120.1, 118.5, 112.3. ^{31}P NMR (162 MHz, $CDCl_3$) δ (ppm) 33.581. HRMS (MALDI-TOF, *m/z*) calcd for $C_{32}H_{19}N_2OP[M+H]^+$, 479.1313, found 479.1327.

*Synthesis of 5-phenyl-7,7-di-p-tolyl-5,7-dihydroindeno[2,1-b]carbazole (**i-iCz**)*

To a solution of **1** (1.96 g, 5 mmol) in toluene (50 mL), *p*-tolylmagnesium bromide (1 M in ether, 10 mL) was added slowly at room temperature under an argon atmosphere. Then the mixture of the reaction was heated to reflux and kept overnight. After cooling to room temperature, the reaction mixture was filtered off and the filtrate was extracted with EtOAc and brine. The resulting organic layer was dried over $MgSO_4$, and the solvent was removed by rotavapor to give the crude intermediate **2**. Subsequently, AcOH/HCl (10 mL/1mL) was added slowly into the resulting intermediate **2** and stirred at room temperature for 10 minutes. Then the reaction mixture was extracted with chloroform and brine. The resulting organic layer was dried over $MgSO_4$ and the solvent was removed by rotavapor. The crude product was then purified by column chromatography (chloroform/hexane = 1/5) to afford **i-iCz** as white solid (1.54 g, 60%). mp: 258-260 °C. ^{1}H NMR (400 MHz, $CDCl_3$) δ (ppm) 7.85-7.83 (d, J=8 Hz, 1H), 7.71-7.69 (d, *J* = 8.0 Hz, 1H), 7.61-7.53 (m, 4H), 7.49-7.39 (m, 8H), 7.37-7.11 (m, 4H), 6.99-6.97 (d, *J* = 8.0 Hz, 4H), 6.91-6.87 (m, 1H). 2.22 (s, 6H). ^{13}C NMR (101 MHz, $CDCl_3$) δ (ppm) 154.18, 147.09, 141.69, 141.55, 140.38, 138.62, 137.62, 136.06, 133.44, 129.87, 128.91, 128.78, 127.83, 127.78, 127.09, 126.32, 125.53, 125.44, 125.31, 122.09, 120.79, 119.16, 118.74, 118.08, 109.64, 109.19, 65.34, 20.93. HRMS (MALDI-TOF, *m/z*) calcd for $C_{39}H_{29}N[M]^+$, 511.2300, found 511.2294.

*Synthesis of 5-phenyl-12,12-di-p-tolyl-5,12-dihydroindeno[1,2-c]carbazole (**o-iCz**)*

To a solution of **1** (1.96 g, 5 mmol) in toluene (50 mL), *p*-tolylmagnesium bromide (1 M in ether, 10 mL) was added slowly at room temperature under an argon atmosphere. Then the reaction mixture was heated to reflux and kept overnight. After cooling to room temperature, the reaction mixture was filtered off and the filtrate was extracted with EtOAc and brine. The resulting organic layer was dried over $MgSO_4$, and the solvent was removed by rotavapor to give the crude intermediate **2**. Subsequently, HCl (5mL) was added slowly into the resulting intermediate **2** and stirred at room temperature for 10 minutes, followed by extraction with chloroform and brine. The resulting organic layer was dried over $MgSO_4$, and the solvent was removed by rotavapor. The crude product was then purified by column chromatography (chloroform/hexane = 1/10) to afford ***o-iCz*** as white solid (357 mg, 14%). mp: 235-237°C. ^{1}H NMR (400 MHz, $CDCl_3$) δ (ppm) 8.47 (s, 1H), 8.20-8.18 (d, *J* =8.0 Hz, 1H), 7.89-7.88 (d, *J* = 4.0 Hz, 1H), 7.57-7.19 (m, 12H), 7.11-7.09 (d, *J* = 8.0 Hz, 4H), 7.01-6.99 (d, *J* = 8.0 Hz, 4H). 2.27 (s, 6H). ^{13}C NMR (101 MHz, $CDCl_3$) δ (ppm) 151.25, 150.84, 143.76, 141.48, 141.26, 140.53, 137.58, 135.00, 133.18, 129.81, 128.85, 128.10, 127.37, 127.29, 126.97, 126.67, 126.07, 125.80, 123.36, 123.28, 120.19, 120.01, 119.43, 111.30, 109.81, 107.48, 64.76, 20.91. HRMS (MALDI-TOF, *m/z*) calcd for $C_{39}H_{29}N[M]^+$, 511.2300, found 511.2294.

Acknowledgements

This work was supported by the National Science and Technology Council (NSTC), Taiwan, under Grant Nos. 110-2113-M-002-008-MY3, and 111-2113-M-002-026. We also thank the mass spectrometry technical research services from the NTU Consortia of Key Technologies.

Supplementary Material

Supplementary data associated with this article is available in the Supplementary Material.

References

1. Tao, Y.; Yuan, K.; Chen, T.; Xu, P.; Li, H.; Chen, R.; Zheng, C.; Zhang, L.; Huang, W. *Adv. Mater.* 2014, *26*, 7931-7958. https://doi.org/10.1002/adma.201402532
2. Uoyama, H.; Goushi, K.; Shizu, K.; Nomura, H.; Adachi, C. *Nature* 2012, *492*, 234-238. https://doi.org/10.1038/nature11687
3. Yang, Z.; Mao, Z.; Xie, Z.; Zhang, Y.; Liu, S.; Zhao, J.; Xu, J.; Chi, Z.; Aldred, M. P. *Chem. Soc. Rev.* 2017, *46*, 915-1016. https://doi.org/10.1039/C6CS00368K
4. Kaji, H.; Suzuki, H.; Fukushima, T.; Shizu, K.; Suzuki, K.; Kubo, S.; Komino, T.; Oiwa, H.; Suzuki, F.; Wakamiya, A.; Murata, Y.; Adachi, C. *Nat. Commun.* 2015, *6*, 8476. https://doi.org/10.1038/ncomms9476
5. Cui, L.-S.; Nomura, H.; Geng, Y.; Kim, J. U.; Nakanotani, H.; Adachi, C. *Angew. Chem.* 2017, *56*, 1571-1575. https://doi.org/10.1002/anie.201609459
6. Wang, X.; Wang, S.; Lv, J.; Shao, S.; Wang, L.; Jing, X.; Wang, F. *Chem. Sci.* 2019, *10*, 2915-2923. https://doi.org/10.1039/C8SC04991B
7. Zeng, W.; Lai, H.-Y.; Lee, W.-K.; Jiao, M.; Shiu, Y.-J.; Zhong, C.; Gong, S.; Zhou, T.; Xie, G.; Sarma, M.; Wong, K.-T.; Wu, C.-C.; Yang, C. *Nat. Commun.* 2018, *30*, 1704961. https://doi.org/10.1002/adma.201704961
8. Lin, T.-A.; Chatterjee, T.; Tsai, W.-L.; Lee, W.-K.; Wu, M.-J.; Jiao, M.; Pan, K.-C.; Yi, C.-L.; Chung, C.-L.; Wong, K.-T.; Wu, C.-C. *Adv. Mater.* 2016, *28*, 6976-6983. https://doi.org/10.1002/adma.201601675
9. Yi, C.-L.; Lin, C.-Y.; Tang, Y.; Wang, C.-Y.; Huang, C.-W.; Gong, X.; Gong, S.; Wu, C.-C.; Wong, K.-T. *Adv. Opt. Mater.* 2022, 10, 2101791. https://doi.org/10.1002/adom.202101791
10. Ahn, D. H.; Kim, S. W.; Lee, H.; Ko, I. J.; Karthik, D.; Lee, J. Y.; Kwon, J. H. *Nature Photonics* 2019, *13*, 540-546. https://doi.org/10.1038/s41566-019-0415-5
11. Chen, Y.-K.; Jayakumar, J.; Hsieh, C.-M.; Wu, T.-L.; Liao, C.-C.; Pandidurai, J.; Ko, C.-L.; Hung, W.-Y.; Cheng, C.-H. *Adv. Mater.* 2021, *33*, 2008032. https://doi.org/10.1002/adma.202008032

12. Wu, T.-L.; Huang, M.-J.; Lin, C.-C.; Huang, P.-Y.; Chou, T.-Y.; Chen-Cheng, R.-W.; Lin, H.-W.; Liu, R.-S.; Cheng, C.-H. *Nature Photonics* 2018, *12*, 235-240. https://doi.org/10.1038/s41566-018-0112-9
13. Sarma, M.; Wong, K.-T. *ACS Appl. Mater. Interfaces* 2018, *10*, 19279-19304. https://doi.org/10.1021/acsami.7b18318
14. Zhang, M.; Zheng, C.-J.; Lin, H.; Tao, S.-L. *Mater. Horiz.* 2021, *8*, 401-425. https://doi.org/10.1039/D0MH01245A
15. Sarma, M.; Chen, L.-M.; Chen, Y.-S.; Wong, K.-T. *Mater. Sci. Eng. R Rep.* 2022, *150*, 100689. https://doi.org/10.1016/j.mser.2022.100689
16. Wang, M.; Huang, Y.-H.; Lin, K.-S.; Yeh, T.-H.; Duan, J.; Ko, T.-Y.; Liu, S.-W.; Wong, K.-T.; Hu, B. *Adv. Mater.* 2019, *31*, 1904114. https://doi.org/10.1002/adma.201904114
17. Hu, Y.-C.; Lin, Z.-L.; Huang, T.-C.; Lee, J.-W.; Wei, W.-C.; Ko, T.-Y.; Lo, C.-Y.; Chen, D.-G.; Chou, P.-T.; Hung, W.-Y.; Wong, K.-T. *Mater. Chem. Front.* 2020, *4*, 2029-2039. https://doi.org/10.1039/D0QM00188K
18. Lo, Y.-C.; Yeh, T.-H.; Wang, C.-K.; Peng, B.-J.; Hsieh, J.-L.; Lee, C.-C.; Liu, S.-W.; Wong, K.-T. *ACS Appl. Mater. Interfaces* 2019, *11*, 23417-23427. https://doi.org/10.1021/acsami.9b06612
19. Hung, W.-Y.; Fang, G.-C.; Lin, S.-W.; Cheng, S.-H.; Wong, K.-T.; Kuo, T.-Y.; Chou, P.-T. *Sci. Rep.* 2014, *4*, 5161. https://doi.org/10.1038/srep05161
20. Lim, H.; Shin, H.; Kim, K.-H.; Yoo, S.-J.; Huh, J.-S.; Kim, J.-J. *ACS Appl. Mater. Interfaces* 2017, *9*, 37883-37887. https://doi.org/10.1021/acsami.7b10914
21. Lin, T.-C.; Sarma, M.; Chen, Y.-T.; Liu, S.-H.; Lin, K.-T.; Chiang, P.-Y.; Chuang, W.-T.; Liu, Y.-C.; Hsu, H.-F.; Hung, W.-Y.; Tang, W.-C.; Wong, K.-T.; Chou, P.-T. *Nat. Commun.* 2018, *9*, 3111. https://doi.org/10.1038/s41467-018-05527-4
22. Zhong, D.; Yu, Y.; Song, D.; Yang, X.; Zhang, Y.; Chen, X.; Zhou, G.; Wu, Z. *ACS Appl. Mater. Interfaces* 2019, *11*, 27112-27124. https://doi.org/10.1021/acsami.9b05950
23. Luo, D.; Liao, C.-W.; Chang, C.-H.; Tsai, C.-C.; Lu, C.-W.; Chuang, T.C.; Chang, H.-H. *J. Phys. Chem. C* 2020, *124*, 10175-10184. https://doi.org/10.1021/acs.jpcc.0c00825
24. Wong, K.-T.; Chao, T.-C.; Chi, L.-C.; Chu, Y.-Y.; Balaiah, A.; Chiu, S.-F.; Liu, Y.-H.; Wang, Y. *Org. Lett.* 2006, *8*, 5033-5036. https://doi.org/10.1021/ol061791y
25. Lin, M.-S.; Yang, S.-J.; Chang, H.-W.; Huang, Y.-H.; Tsai, Y.-T.; Wu, C.-C.; Chou, S.-H.; Mondal, E.; Wong, K.-T. *J. Mater. Chem.* 2012, *22*, 16114-16120. https://doi.org/10.1039/c2jm32717a
26. Cui, L.-S.; Liu, Y.; Yuan, X.-D.; Li, Q.; Jiang, Z.-Q.; Liao, L.-S. *J. Mater. Chem. C.* 2013, *1*, 8177-8185. https://doi.org/10.1039/c3tc31675k
27. Tsai, M.-J.; Huang, W.-L.; Chen, L.-M.; Ruan, G.-L.; Luo, D.; Tseng, Z.-L.; Wong, K.-T. *J. Mater. Chem. C.* 2023, *11*, 1056-1066. https://doi.org/10.1039/D2TC04638E

28. Maddala, S.; Chung, C.-L.; Wang, S.-Y.; Kollimalayan, K.; Hsu, H.-L.; Venkatakrishnan, P.; Chen, C.-P.; Chang, Y. J. *Chem. Mater.* 2020, *32*, 127-138. https://doi.org/10.1021/acs.chemmater.9b02720
29. Pu, Y.-J.; Koyama, Y.; Otsuki, D.; Kim, M.; Chubachi, H.; Seino, Y.; Enomoto, K.; Aizawa, N. *Chem. Sci.* 2019, *10*, 9203-9208. https://doi.org/10.1039/C9SC04262H

